

Consensus transcriptome signature of perineural invasion in pancreatic carcinoma

Ivane Abiatari,¹ Tiago DeOliveira,¹
Vachtang Kerkadze,³ Christian Schwager,⁵
Irene Esposito,^{2,6} Nathalia A. Giese,³ Peter Huber,^{5,7}
Frank Bergman,⁴ Amir Abdollahi,^{5,7,8}
Helmut Friess,¹ and Jörg Kleeff^{1,7}

¹Department of General Surgery and ²Institute of Pathology, Technische Universität München, Munich, Germany; Departments of ³General Surgery and ⁴Pathology, University of Heidelberg; ⁵Department of Radiation Oncology, German Cancer Research Center and University of Heidelberg, Heidelberg, Germany; ⁶Institute of Pathology, Helmholtz Zentrum München, Oberschleissheim, Germany; and ⁷Center of Cancer Systems Biology, Department of Medicine, Caritas St. Elizabeth's Medical Center, Tufts University School of Medicine; ⁸Children's Hospital Boston, Vascular Biology Program and Harvard Medical School, Department of Surgery, Karp Family Research Laboratories, Boston, Massachusetts

Abstract

Perineural invasion, the growth of tumor cells along nerves, is a key feature of pancreatic cancer. The cardinal symptom of pancreatic cancer, abdominal pain often radiating to the back, as well as the high frequency of local tumor recurrence following resection are both attributed to the unique ability of pancreatic tumor cells to invade the neuronal system. The molecular mechanisms underlying the neuroaffinity of pancreatic tumors are not completely understood. In this study, we developed a novel method to monitor *ex vivo* perineural invasion into surgically resected rat vagal nerves by different human pancreatic tumor cell lines. Genome-wide transcriptional analyses were employed to identify the consensus set of genes differentially regulated in all highly nerve-invasive (nerve invasion passage 3) versus less invasive (nerve invasion passage 0) pancreatic tumor cells. The critical involvement

of kinesin family member 14 (KIF14) and Rho-GDP dissociation inhibitor β (ARHGDI β) in perineural invasion was confirmed on RNA and protein levels in human pancreatic tumor specimens. We found significant up-regulation of KIF14 and ARHGDI β mRNA levels in patients with pancreatic cancer, and both proteins were differentially expressed in tumor cells invading the perineural niche of pancreatic cancer patients as detected by immunohistochemistry. Moreover, functional knockdown of KIF14 and ARHGDI β using small interfering RNA resulted in altered basal and/or perineural invasion of pancreatic tumor cells. Our work provides novel insights into the molecular determinants of perineural invasion in pancreatic cancer. The established nerve invasion model and the consensus signature of perineural invasion could be instrumental in the identification of novel therapeutic targets of pancreatic cancer as exemplified by KIF14 and ARHGDI β . [Mol Cancer Ther 2009;8(6):1494–504]

Introduction

The incidence of pancreatic ductal adenocarcinoma (PDAC) almost equals its mortality rate (1), underscoring the fact that this tumor has one of the worst prognoses of all human malignancies. Advances in molecular biology have increased our understanding of the pathophysiology of PDAC. Oncogene mutations such as those of the *K-ras* gene, tumor suppressor gene mutations such as those of the *p53*, *p16*, and *Smad4* genes, altered expression of apoptosis-related genes, down-regulation of metastasis suppressor genes, and overexpression of mitogenic growth factors and their receptors are among the common alterations that influence the behavior of this aggressive malignancy (2).

PDAC is characterized by a dense tumor stroma (desmoplasia), perineural invasion, and early lymph node and liver metastasis (3, 4). Besides systemic spread, perineural invasion is one of the most significant predictors of poor prognosis (3, 5–7). Perineural invasion is a specific route of spread in PDAC. Although it has also been reported in other cancers, the incidence of perineural invasion is in general significantly lower in various other tumors than it is in PDAC (8, 9). Initial infiltration of tumor cells into the retroperitoneal nerve plexus (10) and along the nerves precludes curative resection (11) and is thought to be the major cause of local recurrence after resection. Recognition of the molecular mechanisms of perineural invasion has therefore major implications for surgical and oncologic therapy.

In this study, we established a new method to monitor *ex vivo* perineural invasion. Highly neuroinvasive pancreatic cancer cell clones from three different tumor cell lines were established. The consensus transcriptional profile of highly invasive versus less invasive pancreatic tumor cells

Received 8/6/08; revised 3/16/09; accepted 4/9/09; published OnlineFirst 6/9/09.

Grant support: Deutsche Krebshilfe 107750 (J. Kleeff) and 106997/107689 (A. Abdollahi, P. Huber, and H. Friess), DFG National Priority Research Program SPP1190 (A. Abdollahi, P. Huber, and H. Friess), NASA/NSCOR NNJ04HJ12G (A. Abdollahi and P. Huber), Tumorzentrum Heidelberg-Mannheim (A. Abdollahi, P. Huber, and H. Friess), and Medical Faculty of the University of Heidelberg Medical School (A. Abdollahi).

The costs of publication of this article were defrayed in part by the payment of page charges. This article must therefore be hereby marked *advertisement* in accordance with 18 U.S.C. Section 1734 solely to indicate this fact.

Note: I. Abiatari and T. DeOliveira contributed equally to this work.

Requests for reprints: Jörg Kleeff, Department of General Surgery, Technische Universität München, Ismaningerstr. 22, 81675 Munich, Germany. Phone: 49-89-4140-5098; Fax: 49-89-4140-4870. E-mail: kleeff@gmx.de

Copyright © 2009 American Association for Cancer Research.

doi:10.1158/1535-7163.MCT-08-0755

was generated by genome-wide expression analysis. Among the identified genes, Rho-GDP dissociation inhibitor β (*ARHGDI β*) and kinesin family member 14 (*KIF14*) were selected for subsequent *in vitro* and *in vivo* confirmation analysis.

Materials and Methods

Cell Culture

Panc-1, Colo357, and T3M4 pancreatic cancer cells were routinely grown in RPMI supplemented with 10% FCS, 100 units/mL penicillin, and 100 μ g/mL streptomycin (complete medium). Cells were maintained at 37°C in a humid chamber with 5% CO₂ and 95% air atmosphere.

Selection of Nerve Invasive Clones

Approximately 5 mm sections of the cervical part of rat vagal nerves were dissected under sterile conditions and placed in specifically designed nerve invasion chambers through a 0.7 mm gap in the bottom of the chamber. Chambers were then placed on tissue culture plates containing standard culture medium (Fig. 1). PDAC cell lines were trypsinized and resuspended in culture medium, and these cell suspensions (2×10^6 cells) were poured into the chambers. With this method, pancreatic cancer cells could invade the nerve and pass through the nerve to the culture plate. After appearance of single cells on the plate (2-3 weeks), the chamber was removed and the invasive cells were propagated. This procedure was repeated three times for three cell lines (Panc-1, Colo357, and T3M4); consequently, three "nerve-invasive" pancreatic cancer cell passages/clones were obtained (0, wild-type; 1, 2, 3, nerve invasion passages).

To avoid "pseudo cloning" (appearance of cells in medium 2 from medium 1 without perineural pass), the level of culture medium in the nerve chamber (medium 1) was kept higher than the level of the medium in the plate (medium 2) and was controlled over the whole course of the experiment to exclude leakage of medium/cell suspension from the nerve chamber (Fig. 1). Furthermore, after each passage,

the nerve was removed from the invasion chamber, fixed in formalin, and embedded in paraffin for immunohistochemical visualization of cancer cell invasion in these nerves (Fig. 2A). Rat tendon of the same size was used as a control.

Immunohistochemistry

Paraffin-embedded nerves and human pancreatic tissue sections (3 μ m thick) were subjected to immunostaining as described previously (12). Sections were deparaffinized in Roticlear (Carl Roth) and rehydrated in progressively decreasing concentrations of ethanol. Antigen retrieval was done by boiling with citrate buffer (pH 6.0) for 15 min. Endogenous peroxidase activity was quenched by incubating the slides in methanol containing 3% hydrogen peroxide. The sections were incubated at 4°C overnight with the primary antibodies [pan-cytokeratin, monoclonal antibody, (KL1; Abcam); KIF14, polyclonal antibody (Bethyl Laboratories); and ARHGDI β , polyclonal antibody (Abcam)]. The slides were rinsed with washing buffer and incubated with EnVision+ System labeled polymer horseradish peroxidase anti-mouse antibody or anti-rabbit antibody (DAKO) for 30 min at room temperature. Tissue sections were then washed in washing buffer and subjected to 100 μ L 3,3'-diaminobenzidine-chromogen substrate mixture (DAKO) followed by counterstaining with hematoxylin. Sections were washed, dehydrated in progressively increasing concentrations of ethanol, and mounted with xylene-based mounting medium. Slides were visualized using the Axio-plan 2 imaging microscope (Carl Zeiss Lichtmikroskopie). Additionally, to confirm the specificity of the primary antibodies, tissue sections were incubated in the absence of the primary antibody and with negative control mouse IgG1 (for cytokeratin) or rabbit IgG (for KIF14 and ARHGDI β). Under these conditions, no specific immunostaining was detected.

Matrigel Invasion Assay

Assays were done in a BD Biocoat Matrigel Invasion Chamber with 8 μ m pore size (BD Biosciences) according to the manufacturer's instructions. Matrigel was rehydrated with 500 μ L serum-free cell culture medium and incubated

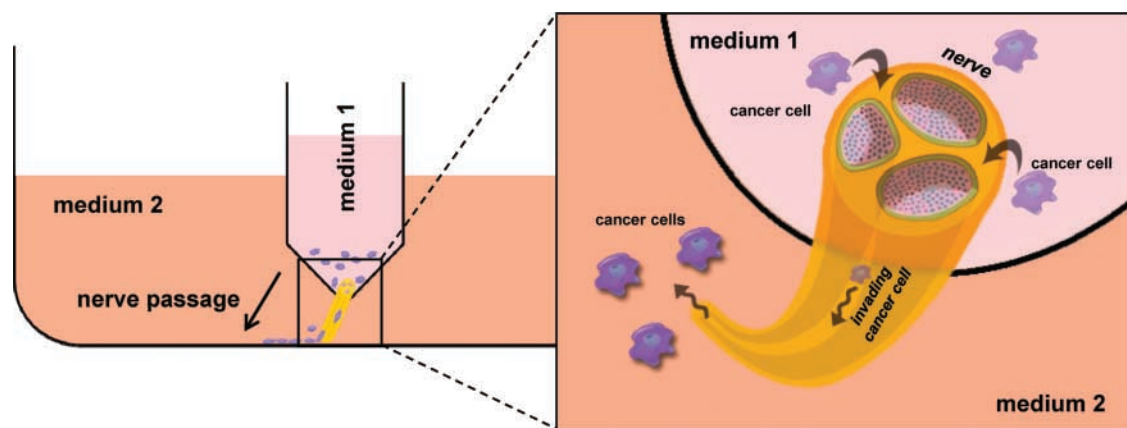


Figure 1. Schematic demonstration of the established *ex vivo* perineural invasion model using rat vagal nerve tissues and pancreatic cancer cell lines as described in Materials and Methods.

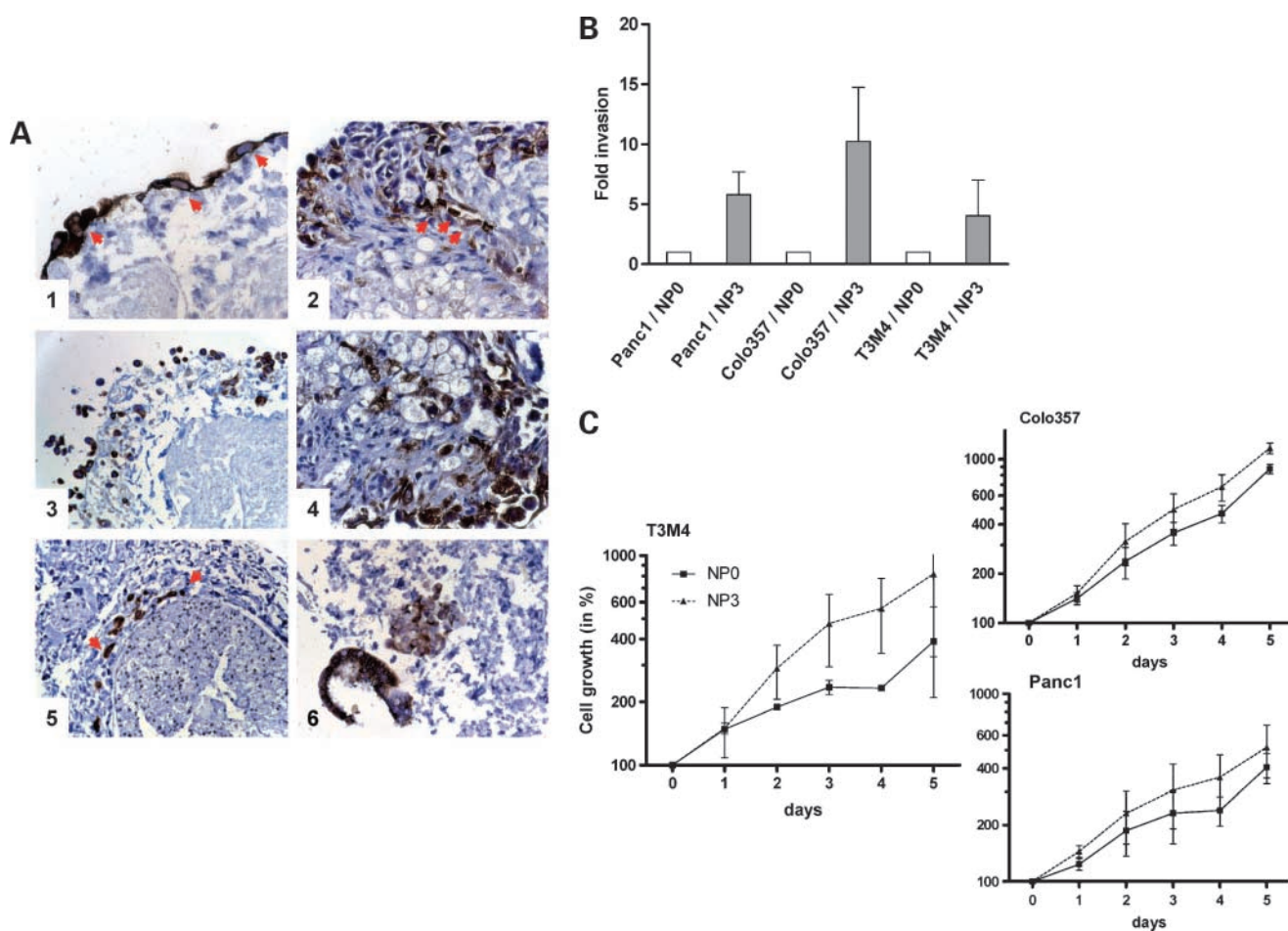


Figure 2. Immunohistochemical staining (brown) of pancreatic cancer cells invading the perineural/neural space of the rat vagal nerves using a pancyctokeratin-specific antibody (A). Tumor cells were visible on the perineural surface (1 arrows, 3) and in the perineural space (5 arrows). Tumor cells also invaded the nerve (2 arrows, 4), occasionally forming duct-like structures (6; bottom left). Matrigel invasion assay showing invasion capacity (B) and 3-(4,5-dimethylthiazol-2-yl)-2,5-diphenyltetrazolium bromide assay for proliferation activity (C) of NP0 and NP3 clones of three pancreatic cancer cell lines. Mean (SD) of triplicate experiments.

in 37°C, 5% CO₂ atmosphere for 2 h, and 5×10^4 cells/mL were added to the top chamber and incubated for 24 h. Cells adhering to the lower surface were fixed with 70% ethanol and stained with Mayer's hematoxylin. The whole membrane was scanned and the invading cells were counted. The assays were done in duplicate and repeated three times.

Proliferation Assay

Anchorage-dependent cell growth was determined by the 3-(4,5-dimethylthiazol-2-yl)-2,5-diphenyltetrazolium bromide colorimetric growth assay (13). Briefly, 2,000 cells per well were plated in 96-well plates and cultured for up to 5 days. Each day cell growth was determined by adding 3-(4,5-dimethylthiazol-2-yl)-2,5-diphenyltetrazolium bromide solution (50 µg/well) for 4 h. Cellular 3-(4,5-dimethylthiazol-2-yl)-2,5-diphenyltetrazolium bromide was solubilized with acidic isopropanol and absorbance was measured at 570 nm. The doubling time was calculated for the exponential growth phase. All experiments were done in triplicate.

Expression Profiling

Genome-wide expression profiling was done using 51K Human Unigene III cDNA microarrays. The microarrays were designed, generated, and hybridized as described previously, with minor modification (14). RNA isolated from pancreatic cell lines was hybridized against universal reference RNA. Linear amplification from 2 µg total RNA was done using the MessageAmp II aRNA Amplification Kit (Ambion). From amplified RNA, 5 µg were used for direct labeling (LabelStar Array Kit; Qiagen) by incorporation of Cy3- or Cy5-UTP (Perkin-Elmer). The corresponding Cy3- and Cy5-labeled probes and competitor DNA [5 µg human Cot-DNA (Invitrogen) and 5 µg poly(dA) (Amersham)] were combined, diluted in hybridization buffer to the final volume of 80 µL (50% formamide, 6× SSC, 0.5% SDS, 5× Denhardt's), and denatured for 5 min at 95°C before hybridization. Prehybridization was done at 42°C for 20 min in 6× SSC, 0.5% SDS, and 1% bovine serum albumin. Slides were rinsed in H₂O and spotted probes were denatured by

incubating the slide for 2 min in 90°C H₂O. Hybridization probe was added and static hybridization was done at 42°C for 16 h. Excess probe was removed by washing in 2× SSC and 0.5% SDS at 42°C for 5 min, in 0.2× SSC and 0.5% SDS at 42°C for 15 min, and finally in isopropanol for 30 s at room temperature. Slides were scanned with the Agilent Microarray Scanner, and image processing was done using the “Chipskipper” software. Data were stored in a MO-MEX database Bloader that enables direct submission of large batches of MIAME-compliant expression profiling data to the ArrayExpress database. Microarray data are available online at ArrayExpress⁹ under the accession number E-TABM-400.

Array Data and Pathway Analysis

Generation of expression matrices, data annotation, filtering, and processing were done using our in-house TableButler software package (14). All microarray statistics, including *t* tests with permutation analysis (*n* = 1000) and cluster analysis, were done using the SUMO software package.¹⁰ Pathway analysis was done based on information available on cellular signaling processes (protein-protein interaction, gene ontology, involvement in specific signaling pathways, cellular localization, etc.) using Pubmed/Entrez gene (National Center for Biotechnology Information),¹¹ Human Protein Reference Database,¹² Gene Ontology Consortium,¹³ and a curated database on signaling networks and systems biology packages (Metacore; Genego)¹⁴ as sources.

Real-time Quantitative Reverse Transcription-PCR

All reagents and equipment for mRNA/cDNA preparation were supplied by Roche Applied Science. mRNA was prepared by automated isolation using the MagNA pure LC instrument and isolation kit I (for cells) and kit II (for tissues). cDNA was prepared using the first-strand cDNA synthesis kit for reverse transcription-PCR (RT-PCR; AMV) according to the manufacturer's instructions. Quantitative RT-PCR (QT-PCR) was carried out using the Light-Cycler FastStart DNA SYBR Green kit. The number of specific transcripts was normalized to the housekeeping gene cyclophilin B and presented as copies/10,000 copies cyclophilin B. For nerve invasion assays, data were normalized to rat GAPDH and expressed as cytokeratin 19 copies/10,000 copies rat GAPDH. All primers were obtained from Search-LC.

Tissue Sampling

Pancreatic tissue specimens were obtained from patients who underwent pancreatic resection or through an organ donor program from previously healthy individuals. Nerve invasion tissue arrays were created from nerve invasion areas of pancreatic cancer and constructed using a manual tissue arrayer (Beecher Instruments). The Human

Subjects Committee of the University of Heidelberg approved all studies. Written informed consent was obtained from all patients.

Small Interfering RNA Transfection

For transient transfection, two different validated small interfering RNAs (siRNA) for KIF14 and ARHGDIβ, respectively, were used (Qiagen; KIF14: siRNA1 ATGGT-TAATCGTGCTCCAGAA and siRNA2 CAGACAT-GATATATCAGATAA and ARHGDIβ: siRNA1 AATACGTTTCAGCACACCTACA and siRNA2 AAG-GAAGGTTCTGAATATAGA). siRNA (5 μg/well) were transfected using RNAi-Fect (Qiagen) as transfection reagent in 6-well plates. Scrambled siRNA was used for control. Functional experiments were done after 48 h of siRNA transfection.

Immunoblotting

Protein levels were assessed by immunoblotting as described previously (15) using specific KIF14 and ARHGDIβ antibodies. Densitometry analysis of the blots was done using the ImageJ software (NIH).

Anoikis Assay

Cells were plated at a density of 1 × 10⁵ per well in 12-well plates coated with 2 mL of a 20 mg/mL polyhydroxyethylmethacrylate/ethanol solution (15). After incubation for 72 h under standard culture conditions, the cell suspension was collected and centrifuged at 1,350 rpm for 10 min and then dissolved in 1:4 diluted binding buffer (1 mL binding buffer and 3 mL distilled water). Annexin V-FITC (5 μL; human Annexin kit; Bender MedSystems) were added and vortexed for a few seconds and then incubated for 10 min at room temperature. Cell viability was analyzed by fluorescence-activated cell sorting after adding 10 μL of the 20 μg/mL propidium iodide stock solution (final concentration 1 μg/mL).

Statistical Analysis

Results were expressed as mean ± SE. For statistical analyses, the nonparametric Mann-Whitney *U* test was used unless indicated otherwise. Significance was defined as *P* < 0.05. Statistical analysis of microarray data, including gene set enrichment for gene ontology categories, was done using the SUMO software package and Genego, as described above.

Results

Establishment of Highly Nerve-Invasive Pancreatic Cancer Cell Clones

To create highly nerve-invasive pancreatic cancer cells, an *ex vivo* perineural invasion assay was designed using rat vagal nerves and pancreatic cancer cell lines (Fig. 1). Three nerve-invasive clones (NP1, NP2, and NP3) of Panc-1, Colo357, and T3M4 pancreatic cancer cell lines were obtained from these experiments as described in Materials and Methods. Passage time gradually decreased from the first to the third passage in the nerve invasion assay (from ~25 to 12 days), indicating increased perineural invasiveness of later passages. Immunohistochemical staining for pancytokeratin, which was used as a marker of pancreatic cancer cells, revealed perineural association and migration of cancer

⁹ <http://www.ebi.ac.uk/arrayexpress>

¹⁰ <http://www.MolecularOncology.de>

¹¹ www.ncbi.nlm.nih.gov/entrez

¹² www.hprd.org

¹³ www.geneontology.org

¹⁴ www.genego.com

cells through the nerve (Fig. 2A), similar to what has been observed *in vivo* (10, 11). Neither passing nor invasion of pancreatic cancer cells was observed in the control tendon group (data not shown).

After establishment of highly nerve-invasive clones, the basal invasion capacity of NP3 cells compared with wild-type cells (NP0) was analyzed. Matrigel invasion assays revealed 4.0- to 10.2-fold increased invasion of NP3 cells compared with NP0 cells (Fig. 2B). Analysis of the basal growth of NP0 versus NP3 cells revealed an increased doubling time in T3M4 cells for NP3 (1.4 ± 0.4 days) in comparison with NP0 T3M4 cells (2.5 ± 0.4 days; $P < 0.05$). In contrast, the doubling times of Colo357 and Panc-1 NP3 cells were not significantly different from those of the respective NP0 cells (Fig. 2C).

Consensus Transcriptional Signature of Nerve Invasion

To characterize the molecular mechanisms underlying pancreatic tumor nerve invasion on the transcriptome level, genome-wide expression profilings (51K human cDNA chips) were done. The consensus transcriptional signature of neuroinvasion was generated by searching for significantly regulated genes in all three neuroinvasive versus noninvasive pancreatic cancer cell lines. Using the nonparametric Mann-Whitney test or the *t* test combined with permutation analysis ($n = 1,000$ and standard Bonferroni correction), we found 680 transcripts differentially regulated in all three NP3 versus NP0 pancreatic cancer cell lines ($P < 0.01$). The consensus transcriptional signa-

ture of neuroinvasion is presented as a heat map using hierarchical clustering with Pearson distances and average linkage analysis (Fig. 3A). From among the consensus signature, the 45 up-regulated genes were selected. These are presented in Table 1. KIF14 was the top down-regulated gene in this panel and therefore was analyzed in more detail. The consensus gene signature was further analyzed for enrichment of functional gene categories. The top 10 functional processes affected in the nerve invasion process are presented (Fig. 3B). The *ex vivo* passaging of tumor cells through the nerves resulted in significant enrichment for gene ontology processes such as immune response, transport, membrane trafficking and signal transduction, cytoskeleton reorganization and cell motility, blood coagulation, cell adhesion, and others (Fig. 3B). For further in-depth analysis, we selected ARHGDI β as an important and differentially regulated member of the "cytoskeleton reorganization and cell motility" group.

Characterization of KIF14 and ARHGDI β Expression in Nerve Invasion of Pancreatic Cancer

Because KIF14 and ARHGDI β were identified as nerve invasion-specific genes, the expression of these genes in all nerve passage clones was next analyzed using QRT-PCR. KIF14 down-regulation (Fig. 4A) and ARHGDI β up-regulation (Fig. 4B) were evident in nerve invasive clones of all three pancreatic cancer cell lines, confirming our microarray findings. Although expression of these genes in all NP clones was not significantly different, the tendency of KIF14 down-regulation and ARHGDI β up-regulation from

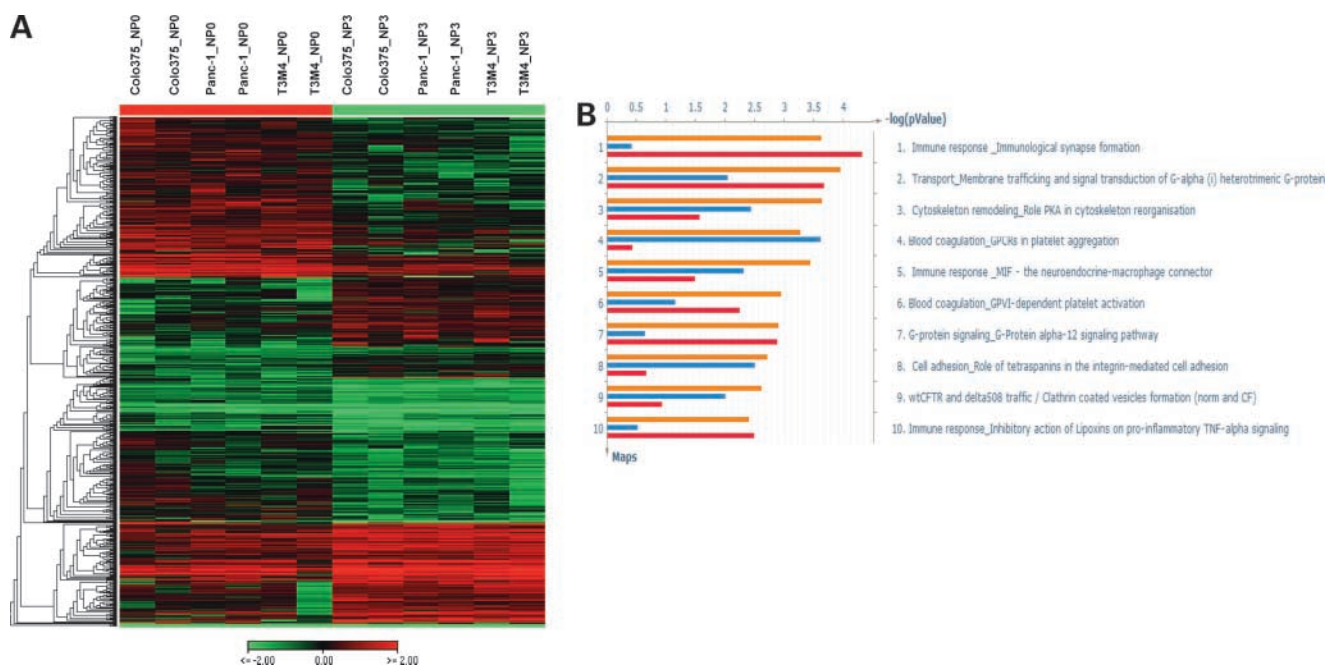


Figure 3. **A**, consensus transcriptome signature of pancreatic neuroinvasion. 680 transcripts were identified to be differentially regulated between nerve invasive NP3 and NP0 cell lines ($P < 0.01$). Each row represents \log_2 expression ratios of an individual gene (pancreatic cell line versus reference RNA), and the columns indicate each respective sample (Colo357, Panc-1, and T3M4 cells). Expression ratios are colored according to the scale bar: *green*, down-regulation; *red*, up-regulation compared with universal reference RNA. **B**, functional categories enriched for genes differentially regulated in nerve invasion (according to GeneGO maps as described in Materials and Methods). Bars are colored based on the regulation of the genes in nerve-invasive NP3 population: all 680 genes (*orange*), genes with nerve invasion up-regulated (*red*), and down-regulated genes (*blue*).

Table 1. Selected genes differentially regulated in all three NPO versus NP3 pancreatic cancer cell lines

Gene name	Gene description	RefSeq	Difference NPO-NP3 (log ₂)
KIF14	<i>Homo sapiens</i> KIF14 mRNA	XM_375825	-9.48
SFRS1	<i>H. sapiens</i> hypothetical gene supported by AK126318 mRNA	XM_375475	-8.68
FLJ34443	<i>H. sapiens</i> hypothetical protein FLJ34443 mRNA	NM_175918	-7.81
ADSSL1	<i>H. sapiens</i> adenylosuccinate synthase-like 1, transcript variant 2, mRNA	NM_152328	-7.46
UNC84A	<i>H. sapiens</i> unc-84 homolog A (<i>Caenorhabditis elegans</i>) mRNA	XM_379766	-6.91
EPS8L2	<i>H. sapiens</i> EPS8-like 2mRNA	NM_022772	-6.87
LOC399959	<i>H. sapiens</i> hypothetical gene supported by BX647608 mRNA	XM_378316	-6.84
YPEL5	<i>H. sapiens</i> yippee protein (CGI-127), mRNA	NM_016061	-5.86
GSTZ1	<i>H. sapiens</i> glutathione transferase ζ1 (maleylacetoacetate isomerase)	NM_145870	-4.81
GNRH1	<i>H. sapiens</i> gonadotropin-releasing hormone 1 (luteinizing-releasing hormone)	NM_000825	-4.75
YPEL1	<i>H. sapiens</i> yippee-like 1 (<i>Drosophila</i>) mRNA	NM_013313	-4.69
YTHDC2	<i>H. sapiens</i> FLJ21940 protein mRNA	NM_022828	-4.38
CLK1	<i>H. sapiens</i> CDC-like kinase 1 mRNA	NM_004071	-4.27
LOC442546	<i>H. sapiens</i> similar to GTF2I repeat domain-containing 1 isoform 2	XM_380014	-4.09
SUMF1	<i>H. sapiens</i> sulfatase modifying factor 1 mRNA	NM_182760	-4.06
RBAF600	<i>H. sapiens</i> retinoblastoma-associated factor 600 mRNA	NM_020765	-3.82
CDH19	<i>H. sapiens</i> cadherin 19, type 2 mRNA	NM_021153	-3.61
KIAA1856	<i>H. sapiens</i> KIAA 1856 protein mRNA	XM_379774	-3.55
COX7C	<i>H. sapiens</i> cytochrome c oxidase subunit VIIc nuclear gene encoding mitochondrial protein	NM_001867	-3.26
PMP22	<i>H. sapiens</i> peripheral myelin protein 22 transcript variant 3 mRNA	NM_153322	-3.03
CAT	<i>H. sapiens</i> catalase mRNA	NM_001752	-2.99
LSM3	<i>H. sapiens</i> LSM3 homologue, U6 small nuclear RNA associated (<i>Saccharomyces cerevisiae</i>) mRNA	NM_014463	2.42
NARG2	<i>H. sapiens</i> NMDA receptor-regulated gene 2 mRNA	NM_024611	2.6
SETMAR	<i>H. sapiens</i> SET domain and mariner transposase fusion gene mRNA	NM_006515	2.64
PREI3	<i>H. sapiens</i> preimplantation protein 3, transcript variant 2 mRNA	NM_199482	3.04
PCBP1	<i>H. sapiens</i> poly(rC) binding protein 1 mRNA	NM_006196	3.05
ITIH4	<i>H. sapiens</i> inter-alpha (globulin) inhibitor H4 (plasma kallikrein-sensitive glycoprotein)	NM_002218	3.38
ARF4	<i>H. sapiens</i> ADP-ribosylation factor 4 mRNA	NM_001660	4.11
DKFZP434O047	<i>H. sapiens</i> DKFZP434O047 protein mRNA	NM_015598	4.49
ADK	<i>H. sapiens</i> adenosine kinase transcript variant ADK-long mRNA	NM_006721	4.53
LOC126669	<i>H. sapiens</i> hypothetical protein mRNA	XM_375809	4.64
PDCD11	<i>H. sapiens</i> programmed cell death 11 mRNA	XM_374829	4.78
BRMS1	<i>H. sapiens</i> breast cancer metastasis suppressor 1 mRNA	NM_015399	5.13
SRPRB	<i>H. sapiens</i> signal recognition particle receptor B subunit mRNA	NM_021203	5.16
PME-1	<i>H. sapiens</i> protein phosphatase methylesterase-1 mRNA	NM_016147	5.84
NUDT5	<i>H. sapiens</i> nudix (nucleoside diphosphate-linked moiety X)-type motif 5 mRNA	NM_014142	6.15
DERL2	<i>H. sapiens</i> carcinoma-related gene (F-LANA), mRNA	NM_016041	6.19
WDR12	<i>H. sapiens</i> WD repeat domain 12 mRNA	NM_018256	6.45
MGC3130	<i>H. sapiens</i> hypothetical protein MGC3130 mRNA	NM_024032	6.71
WDR36	<i>H. sapiens</i> T-cell activation WD repeat protein mRNA	NM_139281	6.85
CSF1R	<i>H. sapiens</i> colony stimulating factor 1 receptor	NM_005211	7.02
TRIP13	<i>H. sapiens</i> thyroid hormone receptor interactor 13 mRNA	NM_004237	7.51
KIAA1715	<i>H. sapiens</i> KIAA1715 mRNA	NM_030650	8.09
MAPRE2	<i>H. sapiens</i> microtubule-associated protein RP/EB family, member 2 mRNA	NM_014268	8.68
DKFZp564J157	<i>H. sapiens</i> DKFZp564J157 protein mRNA	NM_018457	12.07

NOTE: Differences in expression are presented as log₂.

NP0 to NP3 was obvious. KIF14 down-regulation and ARHGDIβ up-regulation in nerve invasive clones was also evident on the protein level comparing NP0 versus NP3 clones (except for ARHGDIβ and Panc-1 cells, where protein levels were not appreciably different; Fig. 4A and B, bottom).

Subsequently, we analyzed the expression of KIF14 and ARHGDIβ mRNA in normal pancreatic ($n = 20$), chronic pancreatitis ($n = 20$), and pancreatic cancer ($n = 58$) bulk tissues using QT-PCR. Both KIF14 and ARHGDIβ showed significantly elevated mRNA levels in chronic pancreatitis as

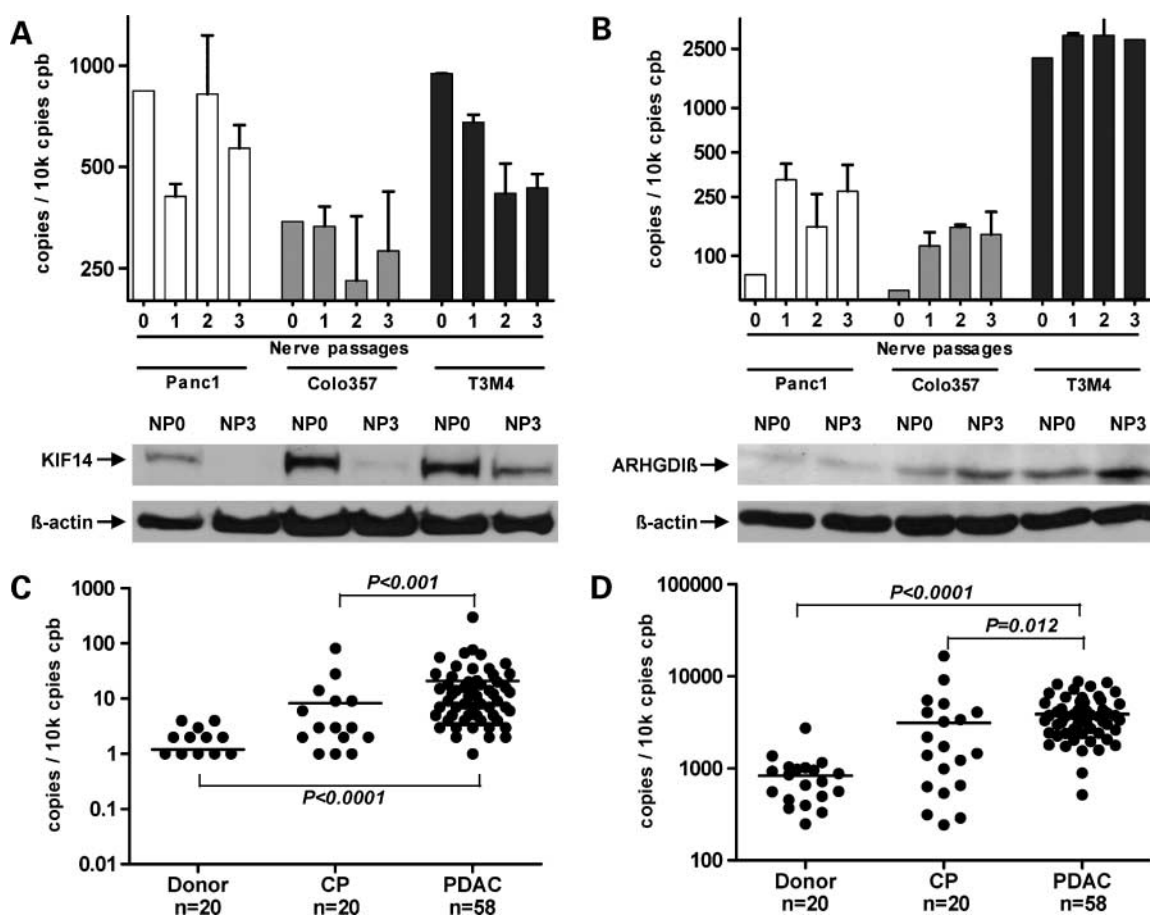


Figure 4. Expression of KIF14 (A) and ARHGDIβ (B) mRNA and protein in nerve passage clones using QT-PCR (top) and immunoblot analysis (bottom) as described in Materials and Methods. Expression of KIF14 (C) and ARHGDIβ (D) mRNA in normal pancreatic tissues ($n = 20$) as well as chronic pancreatitis ($n = 20$) and pancreatic cancer ($n = 58$) bulk tissues using QT-PCR as described in Materials and Methods. Mean (SD) for A and B. Horizontal lines (C and D) represent the mean expression level.

well as in pancreatic cancer tissues (Fig. 4C and D). We investigated the localization of these proteins in pancreatic cancer tissues. KIF14 was expressed in cancer cells and nerves of PDAC tissues as well as in islets (Fig. 5A and B).

We further analyzed KIF14 expression in a tissue array panel of microdissected nerve invasive cancer cells. Interestingly, KIF14 was strongly expressed in cancer cells (75% of the analyzed PDAC tissues; $n = 16$) that did not invade nerves (Fig. 5A). In contrast, expression of KIF14 was lost in pancreatic cancer cells that invaded nerves in 62% of the analyzed cases ($n = 37$; Fig. 5B). This difference in KIF14 staining of the cancer cells between nerve invasion and no nerve invasion was statistically significant (Fisher's exact test; $P < 0.05$).

ARHGDIβ expression was predominantly observed in inflammatory and stromal cells (Fig. 5C), explaining in part the observed up-regulation of ARHGDIβ mRNA in bulk pancreatic cancer tissues (Fig. 4D). Expression of ARHGDIβ was absent in the majority of pancreatic cancer cells that did not invade nerves (9 of 10 cases; Fig. 5C). However, ARHGDIβ expression was clearly present in the cancer cells of 67% of the samples in which cancer cells invaded nerves ($n = 64$; Fig. 5D). This switch of ARHGDIβ staining of the cancer

cells between nerve invasion and no nerve invasion was highly statistically significant (Fisher's exact test; $P < 0.001$).

Functional Characterization of KIF14 and ARHGDIβ in T3M4 Pancreatic Cancer Cells

To assess the functional relevance of KIF14 and ARHGDIβ in pancreatic cancer, endogenous expression levels of these proteins were down-regulated in T3M4 pancreatic cancer cells using siRNA. T3M4 was chosen because this cell line revealed the clearest tendency toward KIF14 and ARHGDIβ changes in NP clones and the highest sensitivity to siRNA silencing (Fig. 6A). The basal invasion capacity of transfected cells was analyzed using Matrigel invasion assays. Down-regulation of KIF14 in T3M4 cells using two specific siRNA molecules resulted in 2.23 ± 0.57 -fold ($P < 0.05$) and 2.44 ± 1.03 -fold ($P < 0.05$) increased invasiveness in these cells, respectively. However, there were no significant changes in invasion capacity of ARHGDIβ silenced cells for both siRNAs (1.30 ± 0.42 - and 0.75 ± 0.15 -fold; Fig. 6B).

Next, we analyzed anchorage-independent survival of transfected cells using two specific siRNAs for KIF14 and ARHGDIβ, respectively. Anoikis assay revealed significantly

higher survival ability of KIF14 silenced cells ($167.2 \pm 25.82\%$ and $191.9 \pm 40.64\%$ of control levels) after 72 h (both $P < 0.05$). Down-regulation of ARHGDI β did not display remarkable changes in survival of T3M4 cells ($111.1 \pm 52.40\%$ and $113.0 \pm 6.97\%$; Fig. 6C).

Finally, we sought to analyze the nerve invasion ability of KIF14- and ARHGDI β -transfected T3M4 pancreatic cancer cells using the same siRNAs as described for the basal invasion experiments. Human cytokeratin 19 was used as a marker for epithelial (cancer) cells. After nerve/cancer cell incubation, nerves were removed from the chambers and snap-frozen in liquid nitrogen. Following homogenization and RNA isolation, expression of cytokeratin 19 was quantified in nerve extracts using QT-PCR analysis. This analysis revealed higher expression of cytokeratin 19 mRNA in nerves incubated with KIF14 silenced cells than in control transfected cells, thus showing an increased number of KIF14-transfected cells inside the nerve. In contrast, ARHGDI β -transfected cells displayed reduced nerve invasion ca-

capacity as shown by reduced expression of cytokeratin 19 in nerve homogenates compared with controls (Fig. 6D). This was also confirmed by silencing ARHGDI β in the highly nerve invasive NP3 T3M4 clone, showing markedly reduced nerve invasion compared with control cells (Fig. 6D).

Discussion

In the present study, we provide evidence of a unique transcriptome signature of highly nerve-invasive pancreatic cancer cell lines using a newly developed *ex vivo* perineural invasion model. Two identified genes were further functionally validated and analyzed in a large panel of human pancreatic tissue specimens, confirming their important role in perineural invasion *in vivo*.

Perineural invasion is considered to be a specific path for the spread of pancreatic cancer cells and is thought to be one of the important factors determining local recurrence after resection. In addition, perineural invasion has been

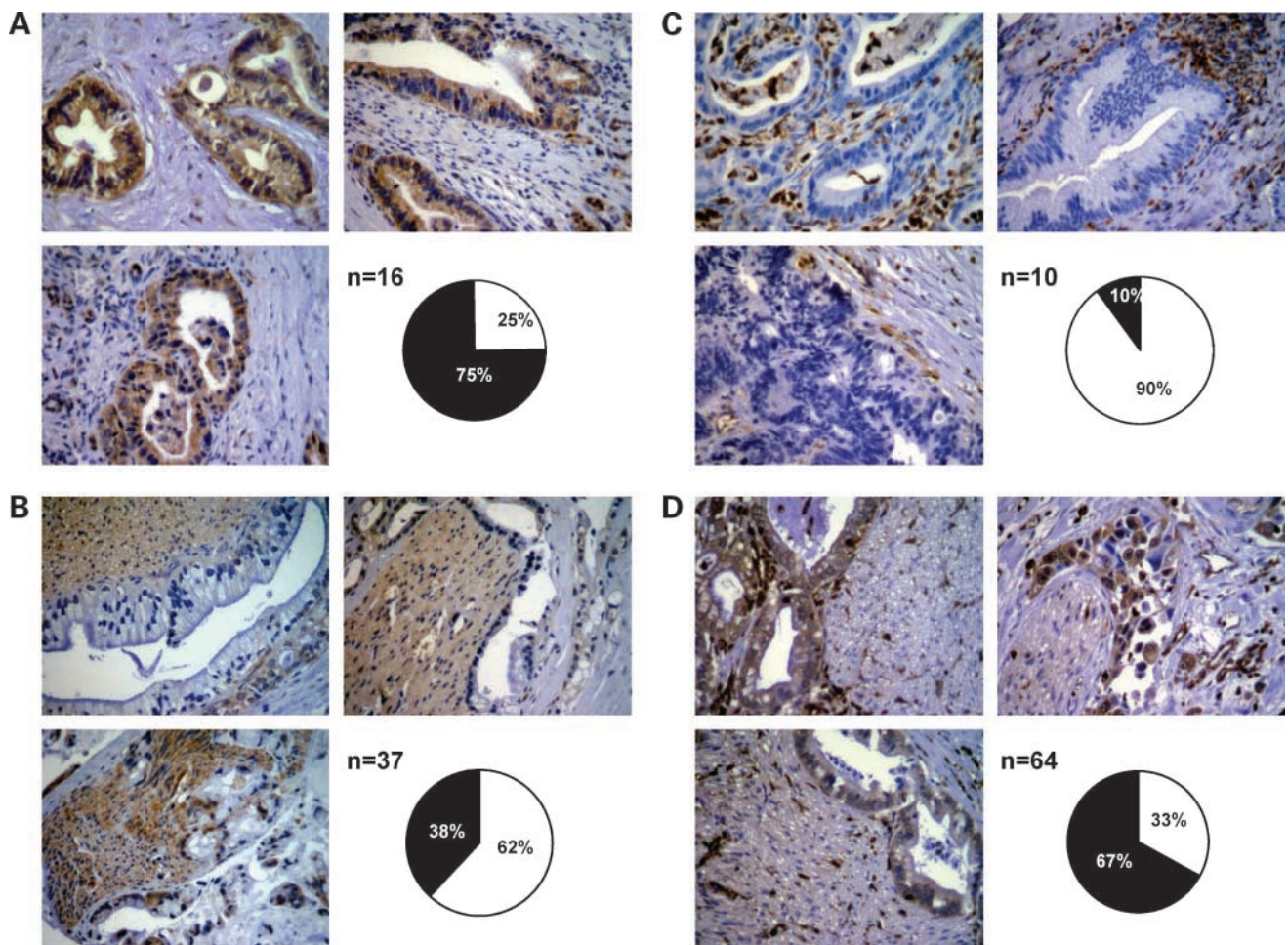


Figure 5. Immunohistochemical staining of pancreatic cancer tissues without (**A** and **C**) and with (**B** and **D**) nerve invasion of cancer cells using KIF14-specific (**A** and **B**) and ARHGDI β -specific (**C** and **D**) antibodies. Percentage of positively stained (+) and negatively stained (-) cancer sections in each group. KIF14- and ARHGDI β -positive cancer cells are shown in **A** and **D**, respectively; absent KIF14 and ARHGDI β expression in the cancer cells is shown in **B** and **C**, respectively.

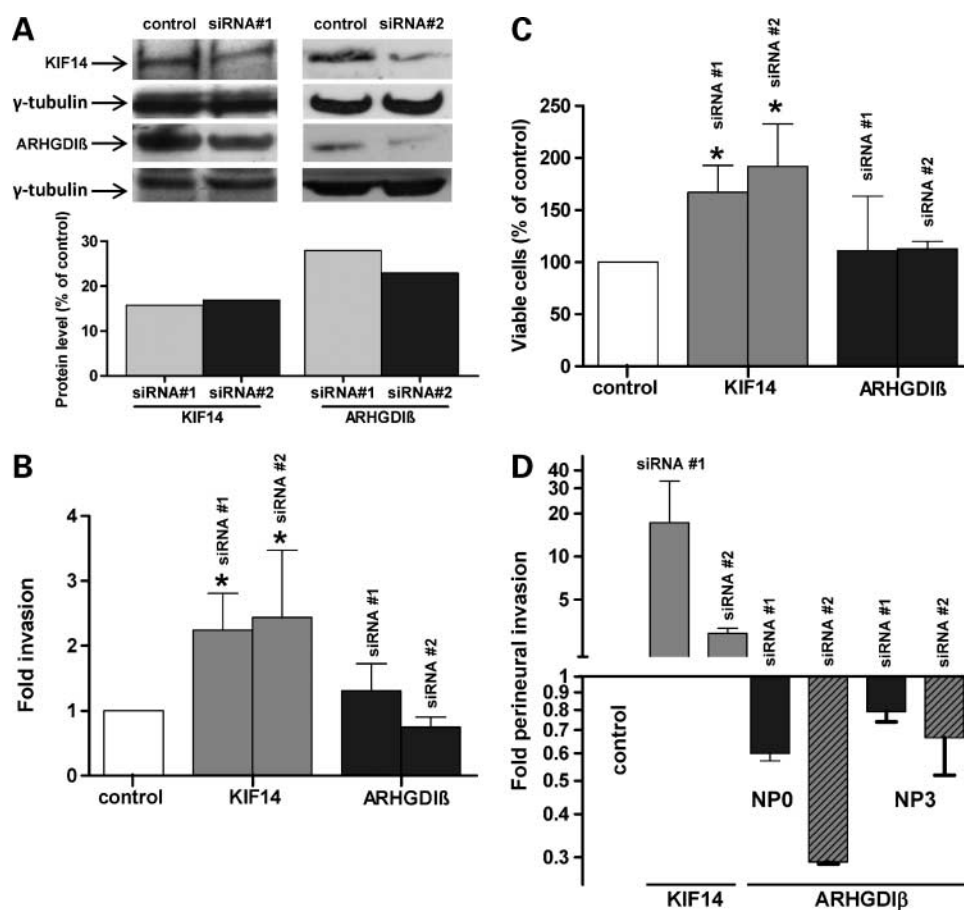


Figure 6. Immunoblot and densitometric analysis, showing down-regulation of KIF14 and ARHGDI β expression in T3M4 pancreatic cancer cells using two specific siRNA molecules (A). Matrigel invasion (B), anoikis (C), and nerve invasion (D) assays in siRNA-transfected versus control-transfected T3M4 cells as described in Materials and Methods. Mean (SD) of three or two (D) independent experiments. *, $P < 0.05$.

implicated in the pain syndrome that affects the majority of PDAC patients (5, 6). A mechanical concept for perineural invasion by pancreatic cancer cells suggests a preferential penetration of tumor cells into the soft perineurium compared with the dense desmoplastic pancreatic tumor microenvironment (8). Another concept is based on the rich vascular and lymphatic supply of the perineural space. According to this theory, the cancer cells within the hypoxic and nutrient-deprived microenvironment grow toward (and along) the nutrient-rich perineural space (8, 16). The neurotropism of pancreatic cancer cells is also attributed to the ability of tumor cells to communicate with perineural and/or neural cells over various neuronal-specific molecules and chemoattractants (3, 8, 17). Although different observations support these concepts, the molecular mechanisms and factors involved in pancreatic cancer cell perineural invasion are not known.

Here, we introduce a novel pancreatic carcinoma perineural invasion model using *ex vivo* perineural implementation of three different human pancreatic cancer cell lines. We found that the resected rat vagal nerves preserve their morphology for >3 weeks under standard cell culture conditions. Moreover, perineural cells (fibroblasts) displayed high viability and proliferation (data not shown). Besides the via-

bility of the nerves, our data also show that their xeno-origin does not affect the efficacy of human pancreatic cells to invade and migrate through the rat nerves. Thus, the key tumor cell-nerve interaction partners are not species dependent.

In two other proposed nerve invasion models for pancreatic cancer, *in vitro* or *in vivo* mouse environments are used to analyze phenotype-specific changes of nerve-invasive human pancreatic cancer cell lines (3, 18). Additionally, these models show significant variability compared with our method, which can be fairly standardized. Our nerve invasion model represents a useful, standardized method for the identification of perineural invasion-related factors and can contribute to better analysis of this phenomenon.

Exposing the characteristic changes linked to perineural invasion, we analyzed the gene expression in highly invasive and minimally invasive pancreatic cancer cell clones. This analysis revealed 680 transcripts that were differentially regulated between these two groups. Among the identified genes, we further investigated KIF14 and ARHGDI β molecules and confirmed their association with perineural invasion in pancreatic cancer.

KIF14 is a mitotic kinesin and a member of the kinesin protein family, which is involved in various biological events such as cargo-containing vesicle transport, mitotic spindle

formation, chromosome segregation, and cytokinesis completion (19, 20). Expression of KIF14 is elevated in mitotic cells (21), and knockdown of this protein leads to multinucleation and apoptosis (21, 22). KIF14 is overexpressed in various malignant diseases, including retinoblastoma and breast and lung cancer, and high expression of this protein correlates with poor outcome in these diseases (23–25). Here, we identified KIF14 as a suppressor of perineural invasion. Analysis of KIF14 expression in a large panel of human pancreatic cancer tissues revealed loss of KIF14 expression in the majority of neural/perineural invading cancer cells, and down-regulation of this protein in pancreatic cancer cells results in enhanced basal and perineural invasion.

In contrast to the protumorigenic role previously proposed for KIF14, our data indicate an anti-invasive function of this gene. Therefore, the observed up-regulation found in other studies might be instead a negative feedback mechanism counteracting tumor invasiveness.

We also identified and characterized ARHGDI β within the consensus perineural invasion signature. ARHGDI β (D4-GDI) is one of the Rho-GDI proteins. These proteins form complexes with members of the Rho family of GTPases and inhibit the dissociation of GDP from Rho proteins, thus preserving the GTPases in an inactive form and preventing their activation by guanine nucleotide exchange factors (26). It has been reported that ARHGDI β is up-regulated in highly invasive breast cancer cells, and its down-regulation leads to reduced invasiveness and reversal to a normal breast epithelial phenotype (27). ARHGDI β has antiapoptotic functions, promoting the resistance of cancer cells to drug-induced toxicity (28).

We show here that down-regulation of ARHGDI β in pancreatic cancer cells did not significantly alter their basal invasion/metastatic capacity or the survival of these cells. However, ARHGDI β was found to be significantly up-regulated in most of the perineural invasive cancer cells of pancreatic cancer tissues *in vivo*, and its silencing led to reduced perineural invasion. Thus, our observations suggest that up-regulation of ARHGDI β in PDAC cells increases perineural invasion of these cells.

Recently, a different model of perineural invasion using highly invasive and minimally invasive pancreatic cell lines also found ARHGDI β , among other factors, to be involved in perineural invasion in pancreatic cancer (18). Independent appearance of ARHGDI β in two different perineural invasion approaches supports the importance of this protein in pancreatic tumor invasion.

The mechanisms by which KIF14 and ARHGDI β induce changes in perineural invasion, as well as the subcellular association of these two proteins in pancreatic cancer, are not known and will be the subject of further studies. Obviously, both molecules directly or indirectly participate in actin organization and cytokinesis, and their deregulation in tumor cells might result in specific cytoskeletal changes essential for perineural invasion in pancreatic cancer.

In summary, we found that changes in the expression of ARHGDI β and KIF14 are associated with perineural invasion in pancreatic cancer. ARHGDI β seems to have a speci-

fic role in perineural invasion of pancreatic cancer, whereas KIF14 might be involved in basal and neural invasiveness of PDAC. The molecular and functional characterization of these two selected proteins supports the reliability of our investigational platform. The consensus transcriptional signature of pancreatic cancer perineural invasion may be instrumental in identification of additional novel markers and therapeutic targets.

Disclosure of Potential Conflicts of Interest

No potential conflicts of interest were disclosed.

Acknowledgments

We thank Barbara Schwager and Claudia Rittmüller for indispensable help with the microarray analysis.

References

- Jemal A, Siegel R, Ward E, et al. Cancer statistics, 2008. *CA Cancer J Clin* 2008;58:71–96.
- Welsch T, Kleeff J, Friess H. Molecular pathogenesis of pancreatic cancer: advances and challenges. *Curr Mol Med* 2007;7:504–21.
- Dai H, Li R, Wheeler T, et al. Enhanced survival in perineural invasion of pancreatic cancer: an *in vitro* approach. *Hum Pathol* 2007;38:299–307.
- Kleeff J, Beckhove P, Esposito I, et al. Pancreatic cancer microenvironment. *Int J Cancer* 2007;121:699–705.
- Tsiotos GG, Farnell MB, Sarr MG. Are the results of pancreatotomy for pancreatic cancer improving? *World J Surg* 1999;23:913–9.
- Sperti C, Pasquali C, Piccoli A, Pedrazzoli S. Survival after resection for ductal adenocarcinoma of the pancreas. *Br J Surg* 1996;83:625–31.
- Conlon KC, Klimstra DS, Brennan MF. Long-term survival after curative resection for pancreatic ductal adenocarcinoma. Clinicopathologic analysis of 5-year survivors. *Ann Surg* 1996;223:273–9.
- Liu B, Lu KY. Neural invasion in pancreatic carcinoma. *Hepatobiliary Pancreat Dis Int* 2002;1:469–76.
- Noto M, Miwa K, Kitagawa H, et al. Pancreas head carcinoma: frequency of invasion to soft tissue adherent to the superior mesenteric artery. *Am J Surg Pathol* 2005;29:1056–61.
- Mitsunaga S, Hasebe T, Kinoshita T, et al. Detail histologic analysis of nerve plexus invasion in invasive ductal carcinoma of the pancreas and its prognostic impact. *Am J Surg Pathol* 2007;31:1636–44.
- Esposito I, Kleeff J, Bergmann F, et al. Most pancreatic cancer resections are R1 resections. *Ann Surg Oncol* 2008;15:1651–60.
- Abiatar I, Kleeff J, Li J, Felix K, Buchler MW, Friess H. Hsulf-1 regulates growth and invasion of pancreatic cancer cells. *J Clin Pathol* 2006;59:1052–8.
- Li J, Kleeff J, Kaye H, et al. Glypican-1 antisense transfection modulates TGF- β -dependent signaling in Colo-357 pancreatic cancer cells. *Biochem Biophys Res Commun* 2004;320:1148–55.
- Abdollahi A, Schwager C, Kleeff J, et al. Transcriptional network governing the angiogenic switch in human pancreatic cancer. *Proc Natl Acad Sci U S A* 2007;104:12890–5.
- Zhang W, Erkan M, Abiatar I, et al. Expression of extracellular matrix metalloproteinase inducer (EMMPRIN/CD147) in pancreatic neoplasm and pancreatic stellate cells. *Cancer Biol Ther* 2007;6:218–27.
- Takahashi T, Ishikura H, Kato H, Tanabe T, Yoshiki T. Intra-pancreatic, extra-tumoral perineural invasion (nex). An indicator for the presence of retroperitoneal neural plexus invasion by pancreas carcinoma. *Acta Pathol Jpn* 1992;42:99–103.
- Zhu Z, Kleeff J, Kaye H, et al. Nerve growth factor and enhancement of proliferation, invasion, and tumorigenicity of pancreatic cancer cells. *Mol Carcinog* 2002;35:138–47.
- Koide N, Yamada T, Shibata R, et al. Establishment of perineural invasion models and analysis of gene expression revealed an invariant chain (CD74) as a possible molecule involved in perineural invasion in pancreatic cancer. *Clin Cancer Res* 2006;12:2419–26.

19. Miki H, Setou M, Kaneshiro K, Hirokawa N. All kinesin superfamily protein, KIF, genes in mouse and human. *Proc Natl Acad Sci U S A* 2001;98:7004–11.
20. Phelps MA, Foraker AB, Swaan PW. Cytoskeletal motors and cargo in membrane trafficking: opportunities for high specificity in drug intervention. *Drug Discov Today* 2003;8:494–502.
21. Carleton M, Mao M, Biery M, et al. RNA interference-mediated silencing of mitotic kinesin KIF14 disrupts cell cycle progression and induces cytokinesis failure. *Mol Cell Biol* 2006;26:3853–63.
22. Gruneberg U, Neef R, Li X, et al. KIF14 and citron kinase act together to promote efficient cytokinesis. *J Cell Biol* 2006;172:363–72.
23. Corson TW, Gallie BL. KIF14 mRNA expression is a predictor of grade and outcome in breast cancer. *Int J Cancer* 2006;119:1088–94.
24. Corson TW, Gallie BL. One hit, two hits, three hits, more? Genomic changes in the development of retinoblastoma. *Genes Chromosomes Cancer* 2007;46:617–34.
25. Corson TW, Zhu CO, Lau SK, Shepherd FA, Tsao MS, Gallie BL. KIF14 messenger RNA expression is independently prognostic for outcome in lung cancer. *Clin Cancer Res* 2007;13:3229–34.
26. DerMardirossian C, Bokoch GM. GDIs: central regulatory molecules in Rho GTPase activation. *Trends Cell Biol* 2005;15:356–63.
27. Zhang Y, Zhang B. D4-GDI, a Rho GTPase regulator, promotes breast cancer cell invasiveness. *Cancer Res* 2006;66:5592–8.
28. Zhang B, Zhang Y, Dagher MC, Shacter E. Rho GDP dissociation inhibitor protects cancer cells against drug-induced apoptosis. *Cancer Res* 2005;65:6054–62.